BIOCHEMISTRY

 Volume 46, Number 38 September 25, 2007

Articles

Stable DNA−Protein Cross-Links Are Products of DNA Charge Transport in a Nucleosome Core Particle†

Chad C. Bjorklund and William B. Davis*

School of Molecular Biosciences, Washington State University, Pullman, Washington 99164-4660

Received March 9, 2007; Revised Manuscript Received July 5, 2007

ABSTRACT: DNA−protein cross-links (DPCs) in nucleosome core particles (NCPs), the fundamental building block of chromatin, arise during times of cellular oxidative stress. These lesions are expected to be detrimental to the cell due to interference with processes like chromatin remodeling, transcription, DNA replication, and epigenetic marking. However, much is still unknown about the mechanisms leading to the formation of DPCs in NCPs, and the exact sites of these lesions in chromatin have not been delineated. During DNA charge transport (CT), an oxidant leads to the formation of a guanine radical cation ($G^{\bullet+}$) which then becomes mobile and migrates away from the initial site of damage. Since previous studies have established that reactions between a $G^{\bullet+}$ and some amino acids lead to DPC formation in both DNA−peptide and DNA−protein complexes, we hypothesized that DNA CT could lead to DPC formation within NCPs. To test this hypothesis, we studied DNA CT reactions in NCPs reconstituted with DNA containing (i) the 601 NCP positioning sequence and (ii) 14 bp of a linker DNA with a covalently attached anthraquinone (AQ) photooxidant. Collectively, the results from Western blotting, EMSAs, and DNA footprinting reactions lead to the conclusion that AQ-initiated DNA CT is responsible for DNA−H3 cross-linking in one specific region of these NCPs. Furthermore, these DPCs are stable for days at 37 °C, indicating that DNA CT in chromatin can lead to long-lived DNA lesions which the cell must somehow find and excise.

Aberrant intracellular oxidation is a ubiquitous problem for aerobic organisms, and under chronic conditions, it is a recognized contributor to diseases like diabetes (*1*), atherosclerosis (*2*), and cancer (*3*). The attack of oxidizing agents on DNA leads to a wide spectrum of mutagenic and/or lethal damage products, including oxidized nucleobase lesions, single- and double-strand breaks, DNA−DNA cross-links, and DNA−protein cross-links (DPCs)[1] (*4*). Even though DPCs are more abundant than either DNA−DNA cross-links or double-strand breaks after cells are exposed to ionizing radiation (*5*), the basic biochemistry of these lesions remains largely unexplored. What is known is that a variety of nuclear proteins can form DPCs in vivo, including nuclear scaffolding proteins, heat shock proteins, and transcription factors (*6*). Intuitively, DPCs in eukaryotic cells commonly involve

† This material is based upon work supported by the National Science Foundation under Career Award 0347270 (W.B.D.) and startup funds provided by Washington State University.

* To whom correspondence should be addressed: School of Molecular Biosciences, Fulmer Hall 275, Washington State University, Pullman, WA 99164-4660. Telephone: (509) 335-4930. Fax: (509) 335-9688. E-mail: wbdavis@wsu.edu.

[1] Abbreviations: AQ, anthraquinone; CT, charge transport; DPC, DNA−protein cross-link; EMSA, electrophoretic mobility shift assay; ExoIII, exonuclease III; $G^{\bullet+}$, guanine radical cation; NCP, nucleosome core particle; $OH^{\bullet}$, hydroxyl radical; Pol III, T4 DNA polymerase III; PyB, pyrimidine band; rNCP, reconstituted nucleosome core particle.

10.1021/bi700475b CCC: $37.00
Published on Web 08/31/2007

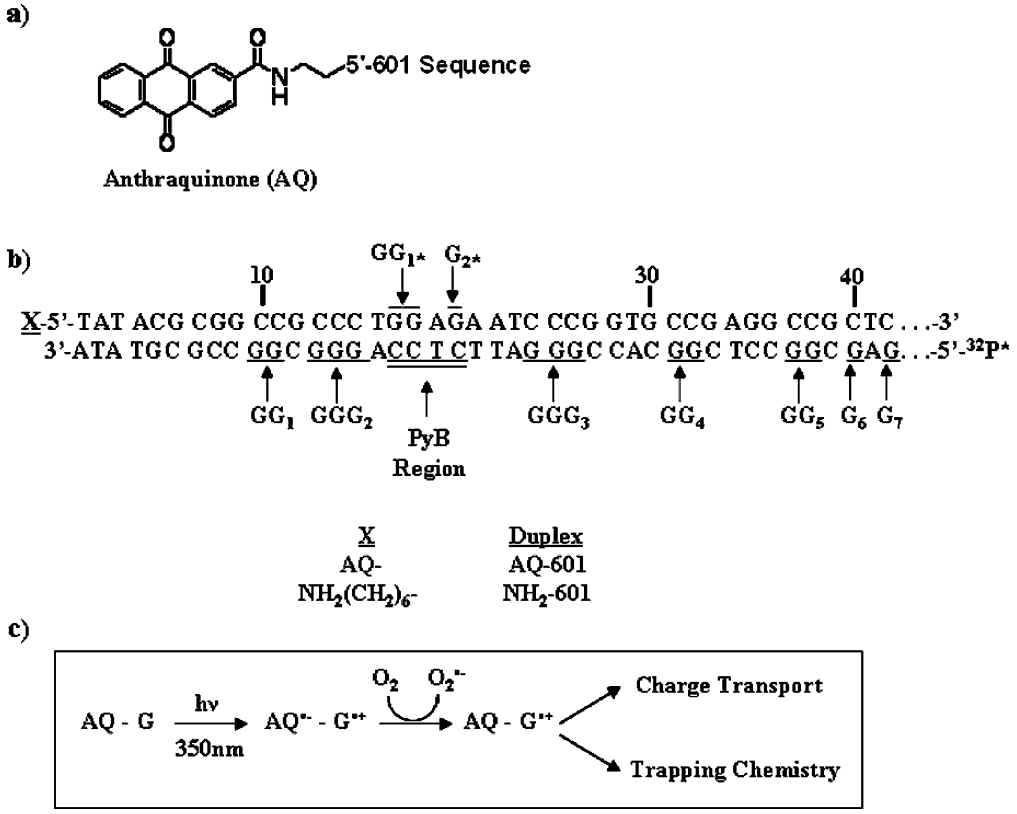

FIGURE 1: Overview of the AQ photooxidant, DNA sequence, and UV-A-induced DNA CT utilized in these studies. (a) Structure of AQ and its covalent attachment to DNA. (b) Sequence of **AQ-601** nearest to AQ. The observed G oxidation sites (GG_1−G_7) and PyB region on the ^{32}P-labeled strand are indicated, as are the G residues (GG_{1*} and G_{2*}) near PyB on the AQ-modified strand. (c) Normal dynamics of DNA CT in AQ-modified DNA duplexes.

proteins bound to DNA in chromatin structures (*6*−*10*) and, in particular, histones H2A, H2B, H3, and H4 which form the octameric protein core of the nucleosome core particle (NCP). Given (i) the importance of the histone proteins in cellular processes like chromatin packaging, transcriptional regulation, and DNA repair and (ii) the propensity of histones to cross-link to DNA, it is surprising that very few reports describing the chemical reactions which lead to DNA−histone cross-links in vivo exist (*11*, *12*), and no reports pinpointing the exact sites of DPC formation within oxidized chromatin exist.

After the oxidation of DNA, one of the most abundant initial products is expected to be the guanine radical cation ($G^{\bullet+}$) since G is the site of lowest oxidation potential within DNA (*13*). Once a $G^{\bullet+}$ is present in DNA, there is a high probability that this electron deficient site, or hole, will migrate through the DNA via a process known as DNA charge transport (CT) (*14*−*17*). During DNA CT, a series of electron transfer reactions between neighboring G residues, or hops, will move the hole ($G^{\bullet+}$) up to 200 Å (20 nm) from the initial site of damage (*18*, *19*). Hole hopping does not continue indefinitely because of competing trapping reactions between $G^{\bullet+}$ and species like H_2O or O_2. Since the rates of hole hopping are faster than these trapping reactions, a steady state distribution of guanine oxidatively induced lesions, including 8-hydroxyguanine and 2,6-diamino-4-hydroxy-5-formamidopyrimidine (Fapy-G), is the typical damage observed after DNA CT (*20*). Recent work has begun to probe the dynamics of DNA CT in typical DNA−protein complexes found in the nucleus. So far, the effect of DNA−protein binding on the guanine damage distribution arising from DNA CT has been fairly minimal in most systems that have been studied (*21*−*23*). However, there have been a few reports of DNA−protein binding leading to a complete inhibition of DNA CT (*22*, *24*) or lower overall levels of guanine oxidatively induced lesions (*25*). These latter studies indicate that we still have much to learn about the dynamics of DNA CT in vivo.

On the basis of recent experiments, there exists the distinct possibility that DNA CT may be one mechanism for the creation of DPCs in chromatin structures. First, it has been observed that chemical reactions between $G^{\bullet+}$ and the amino acids lysine and tyrosine can lead to DPCs between DNA and bound peptides (*26*, *27*) or randomly associated proteins (*28*). Second, DNA CT reactions are not impeded by the formation of NCPs (*23*, *25*), indicating that $G^{\bullet+}$ can be formed in and migrate through the DNA−histone contact regions of chromatin. The synthesis of these prior observations leads us to the central hypothesis of this paper: DNA CT in the NCP can lead to the formation of DNA−histone cross-links. To test this hypothesis, we chose to perform in vitro experiments on model chromatin substrates comprised of NCPs reconstituted with DNA containing the 601 NCP positioning sequence and a well-characterized (*15*) anthraquinone (AQ) photooxidant (Figure 1a). To ensure structural homogeneity in our model NCPs, we used the 601 sequence since it is known for the formation of thermodynamically stable nucleosomes (*29*) with one well-defined structure (*30*). To initiate DNA CT outside of the NCP core, we attached the AQ to the 5′-terminus of a 14 bp DNA linker region. The results of our experiments verify our hypothesis by demonstrating that DNA CT in these NCPs leads to

formation of a DPC between histone H3 and one specific 601 DNA region. Most importantly, these data provide a much needed molecular understanding of where and how DPCs arise in chromatin structures because of DNA oxidative damage.

EXPERIMENTAL PROCEDURES

601 DNA Construction. The 162 bp DNA duplexes **AQ-601** and **NH_2-601** were prepared using PCRs on a pGEM-3z (Promega) plasmid containing the 601 nucleosome binding sequence (Jonathan Widom, Northwestern University, Evanston, IL). The two forward primers, **AQ-F** (AQ-5′-TAT ACG CGG CCG CCC TGG-3′) and **NH_2-F** [NH_2-$(CH_2)_6$-5′-TAT ACG CGG CCG CCC TGG-3′], and one reverse primer, **601-R** (5′-CAC AGG ATG TAT ATA TCT GAC AC-3′), were synthesized at Washington State University on an ABI Applied Biosystems 380B DNA synthesizer. **NH_2-F** was synthesized using a monomethoxytrityl-protected amino linker phosphoramidite (Glen Research), while **AQ-F** was modified at the 5′-terminus by a previously described anthraquinone phosphoramidite (*31*). After synthesis, the primers were deprotected in NH_4OH (40 °C overnight), purified by reverse phase HPLC on a Waters 2690 system equipped with a 996 photodiode array detector and a Nucleosil C18 column (Hichrom), and lyophilized. Primer **AQ-F** was resuspended in water and subjected to ethanol precipitation, while primers **601-R** and **NH_2-F** were first detritylated in 80% acetic acid for 30 min and then ethanol precipitated.

PCRs were performed using the Elongase Enzyme PCR mix (Invitrogen) on a Biometra personal PCR cycler (Biotron). Primers **AQ-F** and **601-R** were used for **AQ-601**, and primers **NH_2-F** and **601-R** were used for **NH_2-601**. The desired 162 bp PCR products were purified using preparative-scale 3% agarose gels. **AQ-601** and **NH_2-601** were labeled with ^{32}P at their free 5′-termini by incubation with T4 polynucleotide kinase (New England Biolabs) and [γ-^{32}P]-ATP (Perkin-Elmer; 5 mCi/mL, specific activity of 3000 Ci/mmol) for 1 h at 37 °C. After chloroform/phenol extraction, the radiolabeled 601 constructs were purified using Probe Quant G50 spin columns (Amersham) followed by ethanol precipitation.

NCP Reconstitution. Chicken erythrocyte NCPs, devoid of avian linker histones H1 and H5, were isolated from chicken erythrocytes (Lampire Biologicals) using a previously reported protocol (*32*). Before reconstitution, the integrity of the core histones was confirmed by visualizing them on an 18% (30:0.5 acrylamide:bisacrylamide) SDS−PAGE gel. Individual reconstitutions of ^{32}P-labeled **AQ-601** and **NH_2-601** into NCPs (forming **rAQ-601** and **rNH_2-601**, respectively) were performed using a previously described protocol (*25*) which results in a 50:1 final concentration ratio of native NCPs to ^{32}P-labeled rNCPs. After reconstitution, the rNCPs were stored at 4 °C in 10 mM sodium phosphate buffer (pH 7.0) until they were needed. NCP reconstitution efficiency was assessed by running 6% native PAGE EMSAs. After drying, these gels were placed into phosphorimaging cassettes (Amersham), and the EMSAs were analyzed by autoradiography using a 445 SI Phosphorimager (Molecular Dynamics) and ImageQuant (Molecular Dynamics).

ExoIII and Hydroxyl Radical Footprinting. Exonuclease III (ExoIII) and hydroxyl radical ($OH^•$) footprinting reactions were used to assess the DNA translational and DNA rotational setting, respectively, in **rNH_2-601** and **rAQ-601**. These reactions were carried out using previously described protocols (*25*). The resulting reaction products were run on 7 M urea, 6% PAGE sequencing gels and analyzed using autoradiography.

UV Irradiation and Assessment of DNA Oxidative Damage. Individual 100 μL samples of naked DNA (100 nM) or rNCPs (100 nM ^{32}P-labeled rNCP, total NCP concentration of 5 μM) in 10 mM sodium phosphate buffer (pH 7.0) were used in all of the experiments reported here. Samples were irradiated for 60 min at room temperature using a Luzchem photoreactor (Luzchem Research) equipped with 10 UV-A lamps (0.3 mW/cm^2 each; 300−390 nm emission). For −UV controls, the rNCP or free DNA samples were kept at room temperature for 60 min on the benchtop under ambient light. Next, all samples were briefly heated to 90 °C to disrupt noncovalent histone−DNA interactions, extracted with phenol and chloroform, and ethanol precipitated in the presence of glycogen. Both irradiated and non-irradiated samples were then dissolved in 10% piperidine and incubated at 90 °C for 30 min. The treated DNA was dried under reduced pressure, washed, and dried twice with ddH_2O, followed by suspension in formamide loading buffer and electrophoresis on 6% acrylamide, 7 M urea sequencing gels. After drying, the gels were analyzed by autoradiography.

SDS−EMSAs. Irradiated and non-irradiated rNCP samples were lyophilized using a speed vac. The dried pellets were then resuspended in 6 μL of 2% SDS and incubated at 50 °C for 1−2 h. The samples were mixed with a glycerol-based SDS loading buffer and electrophoresed on 18%acrylamide (30:0.5) SDS−PAGE gels. The resulting wet gels were analyzed by autoradiography.

Western Blot Analysis. Wet SDS−EMSA gels were transferred to a nitrocellulose membrane by electrophoresing the gel sandwich at a constant current of 200 mA in Western transfer buffer [12.5 mM Tris, 125 mM glycine, 0.1% SDS, and 20% methanol (pH 8.3)]. After the membrane had been blocked with a 10% milk/phosphate-buffered saline/0.05% Tween 20 mixture (milk−PBST) for 1 h at room temperature, the membrane was incubated with primary (rabbit serum) anti-histone antibody (Upstate; 1:5000 dilution) in milk−PBST overnight at 4 °C with slight agitation. The membrane was next washed with PBST (5×, 10 min each), followed by incubation with HRP-conjugated goat anti-rabbit secondary antibody (Upstate; 1:25000 dilution) for 1 h at room temperature with agitation. After the membrane had been washed with PBST, chemiluminescent detection of the histone proteins was carried out using an ECL kit (Pierce) and Omat X-Blue autoradiography film (Kodak).

Pol III Footprinting. ±UV samples were prepared as described above. Immediately after UV irradiation, the histone proteins were degraded in reaction mixtures containing proteinase K (Roche Biochemicals; 60 min at 37 °C). After phenol/chloroform extraction and ethanol precipitation, the DNA was resuspended in 100 μL of 1× Pol III buffer (Fermentas). Five units of Pol III (Fermentas) was added to each sample, and the reaction mixtures were incubated at 37 °C for 3 min. Pol III activity was stopped by phenol/chloroform extraction, followed by DNA ethanol precipita-

tion in the presence of glycogen. The resulting pellet was resuspended in formamide loading buffer and electrophoresed on a 6% acrylamide, 7 M urea DNA sequencing gel. The Pol III products were analyzed by autoradiography of these gels.

Determination of DNA−Protein Cross-Link Lifetimes. **rAQ-601** samples were irradiated for 60 min at room temperature and immediately placed in a 37 °C dry heating block. Aliquots were removed after 0, 1, 3, and 48 h, and the amount of DPCs remaining was assessed by SDS−EMSA analysis (described above).

RESULTS

*Preparation and NCP Reconstitution of Duplexes **AQ-601** and **NH$_2$-601***. The 162 bp duplexes **AQ-601** and **NH$_2$-601** (Figure 1b) were PCR amplified from a pGEM-3z plasmid harboring the 601 sequence (*29*) using forward primers 5′-modified by an AQ photooxidant (Figure 1a) and a NH$_2$-(CH$_2$)$_6$ linker, respectively. **NH$_2$-601** serves as a control duplex in these studies since the amino link is similar in size to AQ but will not undergo any UV-A-induced photochemical reactions (Figure 1c) with DNA. **AQ-601** and **NH$_2$-601** include the 147 bp 601 NCP binding sequence (*33*) and a 14 bp DNA extension proximal to the 5′-modifications. We designed this extension to (i) initiate photooxidation in a region that models B-form linker DNA and (ii) minimize unwanted hydrophobic interactions between AQ and the histone octamer. After PCR and gel purification (Figure 2a), the reverse primer strand in each duplex was 5′-labeled with ^{32}P.

^{32}P-labeled **AQ-601** and **NH$_2$-601** were individually reconstituted onto purified chicken erythrocyte NCPs using a previously published salt-dependent dialysis protocol (*25*). The reconstitution efficiencies of **AQ-601** and **NH$_2$-601** were assessed using electrophoretic mobility shift assays [EMSAs (Figure 2b)] which consistently showed that >95% of the free DNA was incorporated into NCPs to form **rAQ-601** (reconstituted **AQ-601**) and **rNH$_2$-601**.

Structural Characterization of the rNCPs. We interrogated the structure of **rAQ-601** and **rNH$_2$-601** by performing both ExoIII and OH$^\bullet$ footprinting assays (*34*, *35*). The footprinting results for **AQ-601** and **rAQ-601** are shown in Figure 2c, while Figure S1 of the Supporting Information contains the data for **NH$_2$-601** and **rNH$_2$-601**. We carried out these reactions to verify that AQ interacts with the DNA duplex through end capping, as expected from shorter DNA duplexes naked in solution (*31*), and therefore does not interact directly with either the DNA or histones in the nucleosome. First, we used ExoIII, a 3′−5′ exonuclease which will readily cut naked DNA but is known to pause at the entrance to a NCP (*35*). Reaction of both **NH$_2$-601** and **AQ-601** with ExoIII results in identical cutting patterns and the observation of ExoIII activity throughout the 162 bp of DNA. In the rNCPs, ExoIII activity is only observed in the ∼14 bp proximal to the AQ or amino link. Therefore, we conclude that in **rAQ-601** the AQ and its neighboring 14 bp of DNA are free in solution and not protected from ExoIII activity by, for instance, random association of AQ with either the histones or DNA packaged in the core particle.

OH$^\bullet$ footprinting is often utilized to interrogate the rotational setting of nucleosomal DNA, since bound DNA will display an ∼10 bp periodicity of cutting which maps out the orientation of the DNA minor groove with respect to the histone octamer surface (*34*). In free **AQ-601** and **NH$_2$-601**, attack by OH$^\bullet$ leads to semirandom cutting of the DNA duplex (Figure 2c and Figure S1 of the Supporting Information). However, in both **rAQ-601** and **rNH$_2$-601**, an ∼10 bp periodic cutting pattern is observed. The footprints of both rNCPs are identical, and the 10 bp periodicity of cutting indicates that there is only one major rotational setting in these rNCPs. We note that the phased cutting is only observed in the DNA farthest from the AQ 5′-terminus, which indicates that the AQ photooxidant and its proximal DNA are not in contact with the NCP core. Thus, both OH$^\bullet$ and ExoIII footprinting give a consistent picture of the molecular structure of **rAQ-601** which, when coupled with the NCP crystal structure of Davey et al. (*36*) (PDB entry 1KX5), allows us to produce the structural model shown in

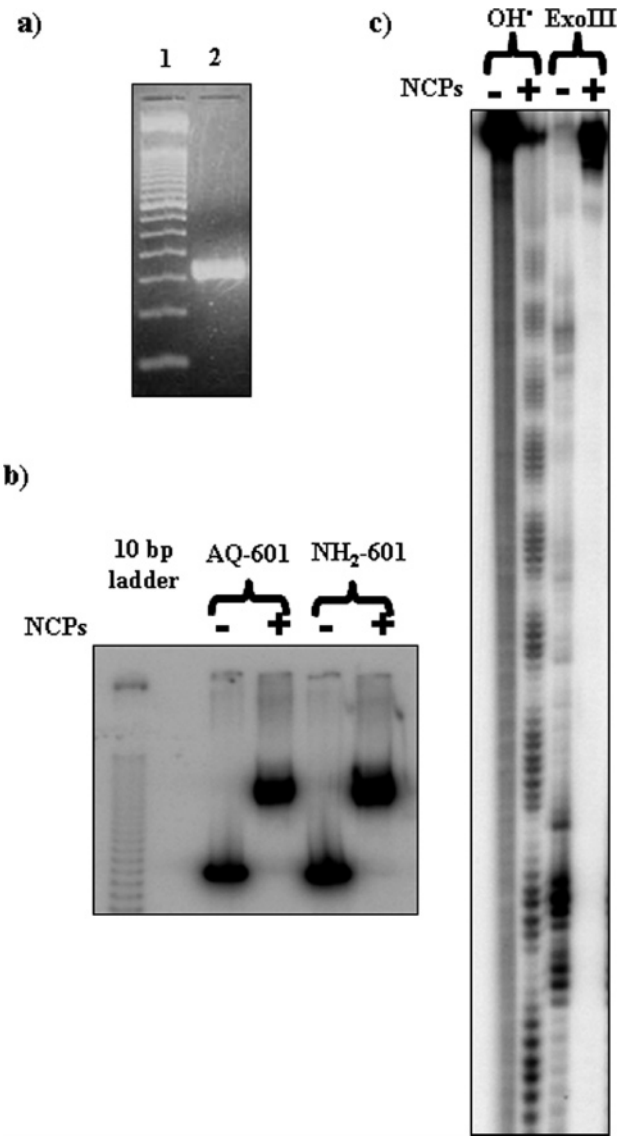

FIGURE 2: Characterization of **AQ-601** and its reconstituted NCPs. (a) Agarose gel (3%) showing a 50 bp DNA ladder (lane 1) and the purified, 162 bp **AQ-601** product obtained by PCR (lane 2). (b) A representative EMSA showing the similar efficiencies (>95%) of reconstitution of **AQ-601** and **NH$_2$-601** into NCPs. (c) Results of OH$^\bullet$ and ExoIII DNA footprinting assays carried out on **AQ-601** and **rAQ-601**.

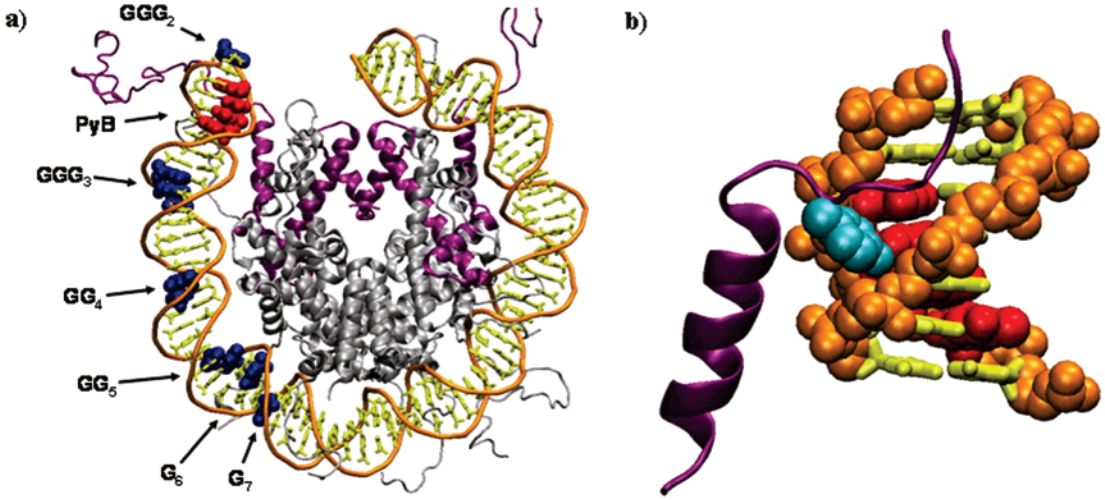

FIGURE 3: Model structure of **AQ-601** rNCPs. (a) Position of the 601 DNA on the histone octamer surface as deduced from a comparison of the results of DNA footprinting on **rAQ-601** (Figure 2) and a high-resolution NCP crystal structure (PDB entry 1KX5). The positions of the observed oxidized G residues (blue), PyB (red), and histone H3 (purple) are indicated. (b) DNA−H3 interface around PyB. The position of the phenoxy side chain of residue H3 Tyr41 (cyan) in the DNA minor groove near PyB is highlighted. Both images were rendered using VMD (www.ks.uiuc.edu/Research/vmd).

Figure 3a. Not shown in this model are the 14 bp overhang and AQ photooxidant.

*DNA Oxidative Damage in UV-Irradiated **AQ-601** and **rAQ-601***. UV-A irradiation of AQ-modified DNA duplexes typically results in the formation of a steady state distribution of guanine oxidatively induced lesions arising from the interplay of (i) DNA hole hopping reactions leading to the migration of the guanine radical cation ($G^{\bullet+}$) and (ii) reactions of $G^{\bullet+}$ with H_2O or other trapping reagents to form irreversible lesions such as 8OG, FapyG, and oxazolone (Figure 1c) (*20*). Treatment of many of these guanine lesions with piperidine leads to a strand break at each oxidized site. Irradiation of **AQ-601**, followed by treatment with hot piperidine, results in the guanine oxidation spectrum shown in Figure 4. CT progresses over 42 bp (∼150 Å, 15 nm) in the naked 601 DNA from the AQ to site G_7 (our nomenclature for the guanine oxidation sites is given in Figure 1b). As controls, neither unirradiated, piperidine-treated **AQ-601** (Figure 4) nor irradiated, piperidine-treated **NH_2-601** (Figure S1 of the Supporting Information) shows any piperidine-induced strand breaks. Therefore, we conclude that DNA oxidation in **AQ-601** arises solely from AQ-induced DNA CT.

The DNA damage distribution arising from UV-A irradiation of **rAQ-601** is shown in Figure 4. Just as in **AQ-601**, DNA CT is efficient all the way out to site G_7 in the rNCPs. We do observe a slight increase in the mobility of the bands corresponding to the 162 bp parent and oxidized GGG_4, GG_5, G_6, and G_7 sequences in **rAQ-601**, but similar gel shifts have been observed previously in DNA CT studies utilizing chicken erythrocyte NCPs (*25*) and are most likely an artifact since the exact magnitude of the shift varies slightly from gel to gel. In the region surrounding GG_1 and GGG_2, the DNA damage spectrum is dramatically different between **AQ-601** and **rAQ-601**. In particular, we note that there are three separate damage bands in the **rAQ-601** samples, while there are only two in **AQ-601**. Using the sequence of **AQ-601** (Figure 1b) and the Maxam−Gilbert G and G+A sequencing lanes in Figure 4, the damage band closest to AQ in the **rAQ-601** lanes appears to be oxidized GG_1. Just as with sites GGG_4−G_7, the yield of damage at site GG_1 is lower in the rNCPs. The most intense damage band in the rNCPs appears to arise from oxidized GGG_2, but why it is so intense in comparison to the other damage bands, especially GG_1, was not clear until after we performed Pol III footprinting assays (see below). The band migrating 20 bp away from the parent band in **rAQ-601** is unique since it is not observed in either irradiated **AQ-601** or irradiated **rNH_2-601** samples (Figure S1 of the Supporting Information). We have named this band PyB, which is short for pyrimidine band, since it does not correlate with any of the Maxam−Gilbert G or G+A sequencing bands in Figure 4. In fact, it arises somewhere in the pyrimidine tract indicated in Figure 1b.

One type of chemistry which we feel that we can strongly rule out for the origin of PyB is the trapping of radical cations at these pyrimidines. Since the oxidation potentials of C and T are higher than that of G (*13*), C (and by inference T) are expected to be only transiently oxidized during DNA CT (*37*) and not serve as radical cation trapping sites. This expectation is substantiated by the observation that piperidine-sensitive pyrimidine oxidation products are observed only during DNA CT in the total absence of guanines (*38*). Since the formation of an oxidized pyrimidine lesion seemed an unlikely origin for PyB, we were forced to consider the possibility that DNA damage other than the typical oxidized nucleobase products was being generated in irradiated **rAQ-601**. Returning to our model of **rAQ-601** in Figure 3a, we expect PyB to lie 3−6 bp inside the entrance of the nucleosome, right near the location where the tail of histone H3 exits the NCP. Since PyB does not appear in **AQ-601**, we next reasoned that these DNA−H3 interactions are necessary for the observation of this band. This line of thinking led us to hypothesize that the PyB band arises from DPCs formed during long-range DNA CT. The following experiments were carried out to test this hypothesis.

*Verification of DPC Formation in Irradiated **rAQ-601** through EMSAs and Western Blotting.* The identification of DPCs has been previously performed using a variety of methodologies (*5*). We turned to denaturing EMSAs (SDS−

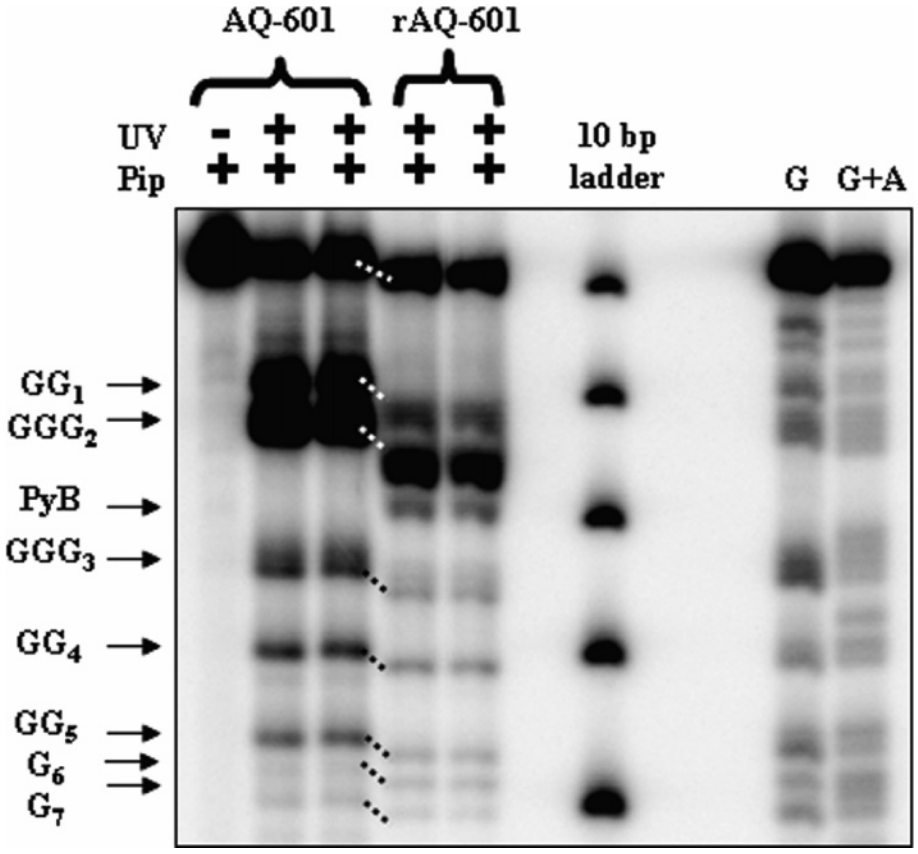

FIGURE 4: Products of DNA CT reactions in **AQ-601** and **rAQ-601**. The positions of piperidine-sensitive oxidation products at sites GG_1-G_7 (Figure 1) were determined by comparisons with the Maxam−Gilbert G and G+A ladders, and the 10 bp DNA ladder (top band, 160 bp). The dotted lines serve as guides between the G oxidation bands in the **AQ-601** and **rAQ-601** samples. The latter bands migrate a bit faster than the former because of an unsystematic gel shift (see the text). Also indicated is the position of the PyB lesion which is only observed in UV-A-irradiated **rAQ-601**.

EMSA) coupled with Western blotting to verify the presence of DNA−histone cross-links in irradiated **rAQ-601** samples and to identify the histone(s) responsible for these reactions. In SDS−EMSAs, any DNA−histone cross-linked complexes are expected to give rise to ^{32}P-containing bands which migrate slower through the gel than native **AQ-601**. We found it necessary to utilize protein denaturing EMSAs in these experiments because of the strong noncovalent interactions between DNA and the histone proteins. Also, we took care to make sure that samples were maintained at temperatures of <50 °C during all manipulations since the PyB band appears on DNA sequencing gels after irradiated **rAQ-601** samples are heated to 90 °C in the absence of piperidine (unpublished experiment). Figure 5a shows autoradiographs of SDS−EMSAs for **NH_2-601**, **AQ-601**, **rNH_2-601**, and **rAQ-601** in the absence and presence of UV irradiation. Note that we observe only the slower-migrating, ^{32}P-labeled products expected from DNA−histone cross-linking in the irradiated **rAQ-601** samples. From autoradiographs of replicate gels, we calculate that the yield of these slower-migrating bands in irradiated **rAQ-601** is 69 ± 7%.

Next, we sought to verify that histone proteins were also present in the slower-migrating SDS−EMSA bands by performing Western blotting on replicate **rAQ-601** SDS−EMSA gels. Each experiment was carried out using a polyclonal antibody raised against one of the four core histones (H2A, H2B, H3, and H4). Prior to use, the ability of each antibody to selectively recognize its appropriate histone antigen was verified. Western blotting was carried out on wet SDS−EMSA gels immediately after autoradiography so that bands visualized using both processes *on the same gel* could be compared and contrasted. Typical Western blots are shown in Figure 5b. In the non-irradiated **rAQ-601** samples, either one (H2A, H2B, or H4) or two (H3) histone bands appear in the Western blots of the four core histones. None of these bands overlap with ^{32}P-labeled **AQ-601** as ascertained by overlaying the results of autoradiography (Figure 5a) and Western blotting (Figure 5b). Therefore, the single band for histones H2A, H2B, and H4 is assigned to free histone monomers. The faster-running band in the H3 Western blots is assigned to the free H3 monomer since it migrates a distance through the denaturing gel comparable to those of the other three histones. We assign the slower-migrating band to H3 dimers since H3 is the only histone with a Cys residue (Cys110), and at the protein concentrations attained during our workup, H3 dimers are commonly observed in the absence of reducing agents (L. Gloss, personal communication).

In the irradiated **rAQ-601** samples, we do not observe any novel, slower-migrating histone bands in Western blots utilizing H2A, H2B, or H4 antibodies. In the anti-H3 Western blot, we do observe a novel histone band in the irradiated **rAQ-601** lane which migrates much slower than either the H3 monomer or H3 dimer bands. In addition, there is a slight increase in band intensity near the H3 dimer band. Both of these slower-migrating H3 bands *exactly* overlap with the slower-migrating ^{32}P-labeled **AQ-601** bands observed in the SDS−EMSA of the irradiated **rAQ-601** samples. Therefore,

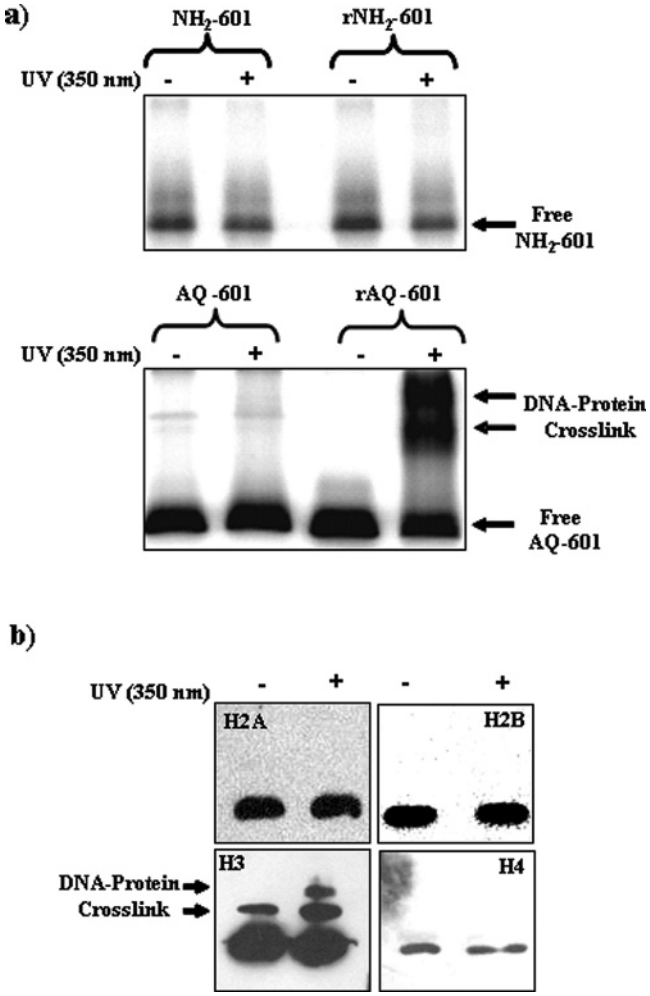

FIGURE 5: DNA−H3 cross-links are generated by DNA CT in **AQ-601** rNCPs. (a) Autoradiographs of SDS−EMSAs performed on **rNH$_2$-601** and **rAQ-601** samples. Only in the UV-A-irradiated **rAQ-601** samples are new, slower-migrating ^{32}P-containing bands observed. (b) Western blots carried out on **rAQ-601** SDS−EMSA gels. Only with anti-H3 antibodies are slower-migrating bands observed on the Western blot. There is complete colocalization of the faster-migrating ^{32}P bands (a) and H3 bands (b) in the irradiated **rAQ-601** samples.

the results of the SDS−EMSA and Western blotting experiments demonstrate that DNA CT in a NCP can lead to the formation of DNA−H3 cross-links.

Pol III Footprinting Identifies the Sites of H3 Cross-Linking in the 601 Sequence. While histone H3 had now been identified as the sole protein involved in DPCs arising from DNA CT in **rAQ-601**, identifying the nucleobases cross-linked to H3 was our next priority. Our earlier analysis of the guanine oxidation products (Figure 4) had revealed the presence of piperidine-sensitive damage in the PyB region of **rAQ-601**, but these experiments were not sufficient to prove that H3−pyrimidine cross-linking was responsible for this damage. Since bulky lesions in DNA like pyrimidine dimers block the 3′−5′ exonuclease activity of Pol III (*39*), we reasoned that the sites of DNA−H3 cross-linking should appear as novel bands in Pol III digests of the irradiated **rAQ-601** samples. Before being treated with Pol III, all samples were treated with proteinase K to digest away the noncovalently bound histone proteins and to trim the DNA−H3 cross-linked complexes so that they would stay in the aqueous layer during a phenol/chloroform extraction. Figure

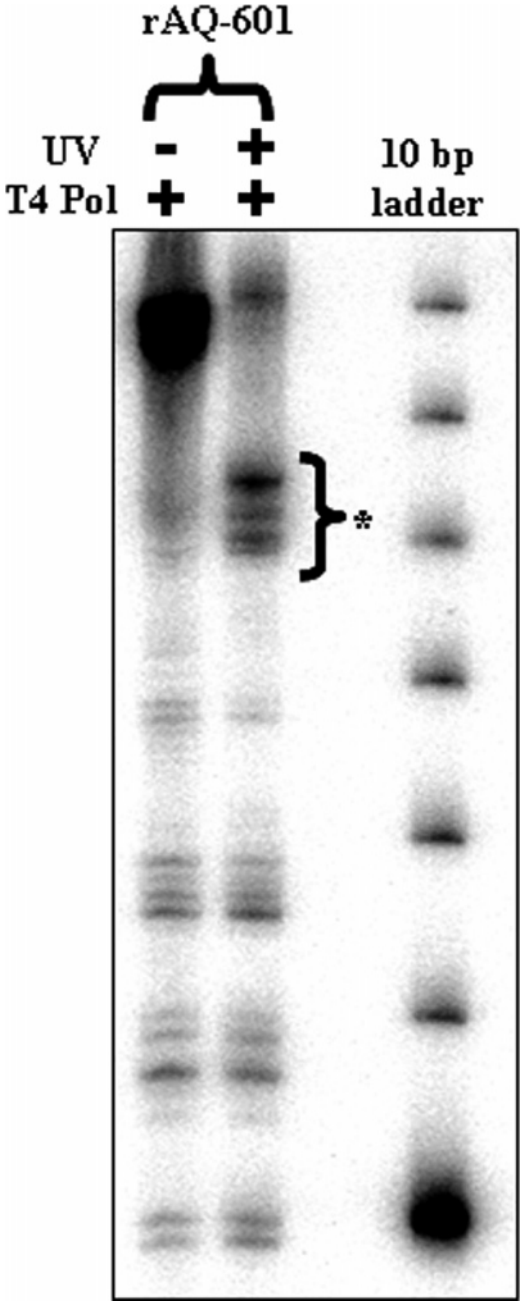

FIGURE 6: Results of Pol III footprinting reactions on non-irradiated and irradiated **rAQ-601** samples with a 10 bp DNA ladder for comparison (most intense band, 100 bp). In the irradiated **rAQ-601** sample, there are new Pol III pause sites observed (asterisks) which are 16−20 bp from the AQ photooxidant.

6 shows the results of these experiments, and indeed, there is one cluster of unique sites where Pol III exonuclease activity is blocked in irradiated **rAQ-601** samples, but not in the non-irradiated **rAQ-601** samples. These new bands do not materialize after Pol III treatment of irradiated **rNH$_2$-601** samples (Figure S2 of the Supporting Information). If one utilizes the 10 bp DNA ladder present in both Figures 4 and 6, it can be seen that the PyB band and one Pol III pause site in irradiated **rAQ-601** arise at the same pyrimidine nucleobase (∼20 bp from the parent band). Furthermore, the most intense Pol III pause site in irradiated **rAQ-601** exactly overlaps with the most intense piperidine band in Figure 4. This indicates that the band we have labeled GGG$_2$ in Figure 4 most likely corresponds to damage at both the GGG tract

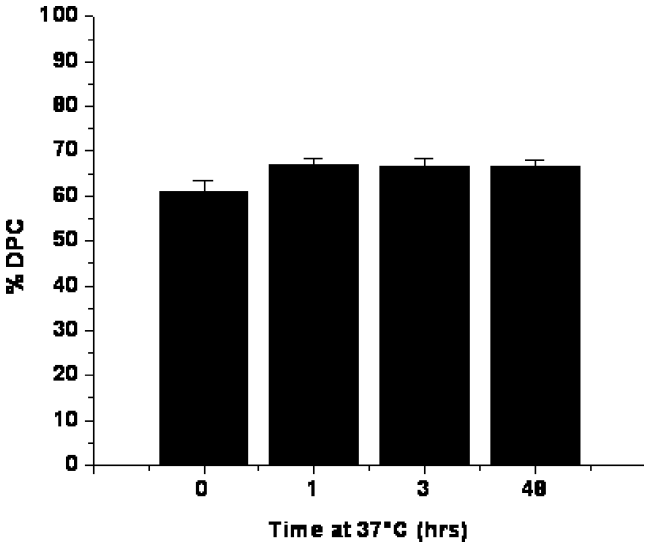

FIGURE 7: Stability at 37 °C of the DNA−H3 cross-links arising from DNA CT in **rAQ-601**. Each % DPC value is an average calculated from three independent SDS−EMSA experiments, and the error bars represent the standard deviation.

and piperidine-sensitive DPCs at the 3′-end of the PyB tract. The higher levels of damage at this location (Figure 4) are consistent with the SDS−EMSAs which showed that a majority of the irradiated **rAQ-601** samples contained DPCs. From these experiments, we conclude that DNA CT in **rAQ-601** leads to the cross-linking of histone H3 and multiple pyrimidines in the PyB region of the 601 sequence.

Lifetime of H3−DNA Cross-Links at 37 °C. Having established the presence of localized H3−DNA cross-links in the irradiated **rAQ-601** samples, we next turned our attention to the stability of these lesions. Previously studied DPCs have demonstrated lifetimes ranging from hours (*40*) to days (*41*). To ascertain the stability of the DNA−H3 lesions formed in this study, we incubated irradiated **rAQ-601** samples at 37 °C for up to 48 h and calculated the amount of DNA−H3 cross-links remaining at each time point from SDS−EMSAs. Figure 7 shows that these cross-links are extremely stable at physiological temperature since their yield does not change even after 48 h.

DISCUSSION

DNA−H3 Cross-Links Are a Product of DNA CT in rNCPs. The studies reported here demonstrate that DNA CT, initiated via the one-electron oxidation of DNA, can lead to the formation of stable DNA−histone cross-links within chromatin structures. Using several different experimental techniques, including DNA footprinting, SDS−EMSA gels, Western blotting, DNA Pol III exonuclease assays, and the visualization of DNA oxidative damage products on sequencing gels, we have shown that reactions between histone H3 and pyrimidine residues (PyB) 3−6 bp into the entrance of **rAQ-601** NCPs are responsible for these cross-links. The Pol III footprinting (Figure 6) and piperidine damageassessment assays (Figure 4) both indicate that the PyB region is the primary, if not only, site of DPC formation in **rAQ-601**. A closer look at our structural model of **rAQ-601** (Figure 3a), generated using our DNA footprinting reactions and a published high-resolution NCP crystal structure, shows that the only histone expected to be in contact with the PyB sequence is histone H3. This prediction is consistent with our Western blotting results which showed that there are no cross-links that include H2A, H2B, or H4 during DNA CT. Furthermore, our model structure shows that PyB is expected to be in contact with the H3 core domain and not the H3 N-terminal tail. This expectation was tested by studying DNA CT in **rAQ-601** samples which had been subjected to limited trypsin digestion (*25*) to remove the histone tails and leave behind residues 27−129 of H3 in the NCP core (*42*). In the absence of the H3 tails, we still observe the presence of the PyB band in irradiated **rAQ-601** (Figure S3 of the Supporting Information), indicating that the majority of H3−DNA cross-linking occurs between the H3 core and the DNA. However, we note that the yield of cross-linking appears to be lower in the tailless rNCPs versus the native rNCPs (Figure S3 of the Supporting Information) since the PyB band:GG_1 intensity ratio is decreased according to autoradiography. The origin of this damage decrease is currently unknown, but we favor the hypothesis that removing the H3 tails lowers the equilibrium constant for DNA binding at the entrance to the nucleosome (*43*, *44*), which would increase the population of unbound PyB-region DNA and thus lower the observed yield of H3−DNA cross-linking.

We have designed **rAQ-601** to possess two key structural elements which help make certain that the chemistry we are observing arises from long-range DNA CT, and not undesirable interactions between the AQ photooxidant and either the DNA or the histone proteins comprising the core particle. The first was the utilization of the 147 bp 601 sequence to ensure that thermodynamically stable, well-positioned rNCPs would be obtained. Second, we placed a 14 bp DNA linker between AQ and the 601 nucleobases at the NCP entrance to help minimize unwanted interactions between AQ and the DNA and histones making up the NCP core. The results of the $OH^{\bullet}$ and ExoIII footprinting reactions are consistent with the intended structure of the **rAQ-601** system. As further evidence of the lack of random AQ−histone or AQ−DNA association, we have manipulated the DNA linker length between AQ and the entrance of the NCP from 10 to 20 bp and not observed any difference in the relative yields of the G oxidation products and PyB (unpublished experiments).

The DNA−histone cross-links formed in **rAQ-601** during DNA CT are not minor damage products, and they are extremely stable at physiological temperatures. Our SDS−EMSA gels indicate that ~69% of all the ^{32}P-labeled **AQ-601** strands in these NCPs are cross-linked to H3 during DNA CT. We note that at first glance this yield of cross-linking appears to be inconsistent with the H3 Western results in Figure 5b, where the DPC bands account for at most 5% of the total signal. However, it must be kept in mind that our NCPs are reconstituted using a 50:1 ratio of chicken erythrocyte NCPs to ^{32}P-labeled 601 DNA. Therefore, the Western blots have a large background signal arising from histone proteins not associated with **AQ-601**, and a quantitative assessment of cross-linking efficiency is not possible from these experiments. The high level of DPC formation in **rAQ-601** implies that oxidized guanines are not expected to be the sole products arising from DNA CT in vivo, and under the right conditions, they may not even be the primary product. This observation has important implications for our earlier study (*25*) of DNA CT in NCPs containing the TG motif. In these prior experiments, we observed that, through

Scheme 1: Proposed Mechanism for DNA−H3 Cross-Linking in **rAQ-601**[a]

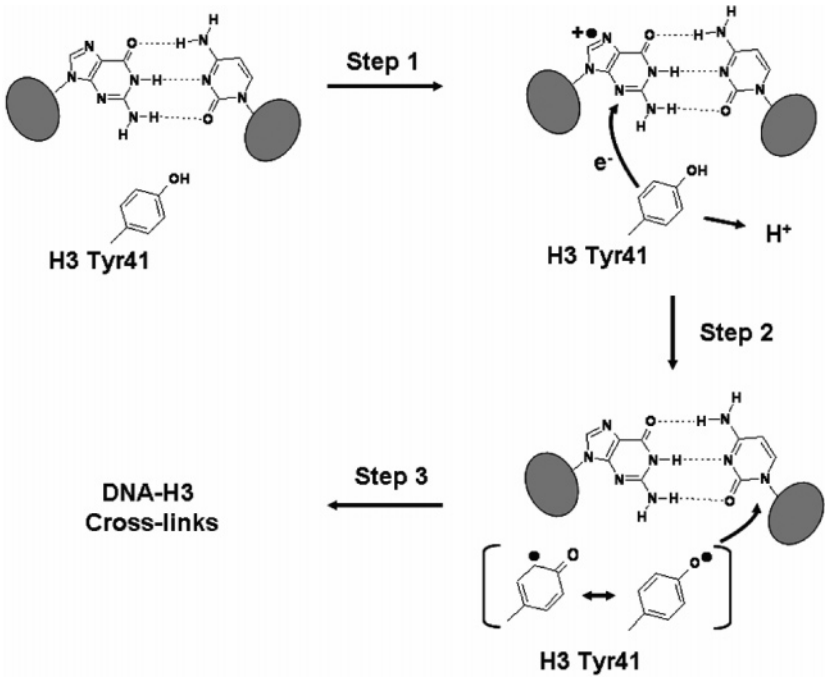

[a] The ovals represent the generic phosphodeoxyribose backbone of DNA, and e^- represents an electron transferred from H3 Tyr41 to a neighboring $G^{\bullet+}$ produced during DNA CT in **rAQ-601**. Attack of the resonance-stabilized Tyr radical is presumed to arise from the C5-centered radical on the left (see the text for details).

an unknown mechanism, the overall yield of guanine oxidatively induced lesions was reduced by ~50% by NCP packaging. If DNA−H3 cross-linking in the TG motif NCPs was also occurring, it would provide an explanation for this phenomenon. Furthermore, it would indicate that DNA−histone cross-links may be a common product of DNA CT in nucleosomes. We are currently reexamining these TG-motif NCPs to test these hypotheses.

Proposed Mechanism for H3−DNA Cross-Link Formation. Since we know the location of PyB in our model NCP structure (Figure 3a), we started interrogating the local DNA−H3 interface for clues about the mechanism of DPC formation. One feature of the PyB region is that the phenol side chain of H3 Tyr41 is in van der Waals contact with the minor groove surface of several PyB base pairs (Figure 3b), a DNA−protein interaction not observed elsewhere in the NCP crystal structure. The buried environment of H3 Tyr41 in the NCP crystal structure is consistent with a previous study (*45*) showing that H3 Tyr41 is protected from reaction with *p*-nitrobenzenesulfonyl fluoride in calf thymus NCPs at our salt concentration. The recognition that H3 Tyr41 is in close contact with the nucleobases in the PyB region allows us to formulate the proposed model for the origin of DNA−histone H3 cross-linking shown in Scheme 1.

In step 1, photoexcitation of AQ initiates DNA CT and this leads to the formation of a $G^{\bullet+}$ near H3 Tyr41. The observation that there are no photoproducts in **rNH$_2$-601** indicates that the AQ photooxidant, and by default the accompanying DNA CT reactions, are absolutely required for DNA−H3 cross-linking. From Figure 1b, sites GG_{1*} and G_{2*} on the AQ-modified strand are located at the location of PyB. Their oxidation during DNA CT is almost certain since we observe guanine oxidation products out to site G_7 in the rNCPs and naked **AQ-601**. Step 2 involves the oxidation of H3 Tyr41 by the neighboring $G^{\bullet+}$. A couple of lines of evidence support this proposed reaction. First, the oxidation potentials of Tyr (E_{ox} = 0.94 V vs NHE) (*46*) and G (E_{ox} = 1.3 V vs NHE) (*47*) make the redox reaction $G^{\bullet+}$ + Tyr-OH → G + Tyr-O$^\bullet$ + H^+ spontaneous. Since H3 Tyr41 and the DNA nucleobases are in close contact, there should be adequate electronic overlap to allow this transfer to occur. Second, electron transfer reactions between $G^{\bullet+}$ and bound amino acids have been observed in small peptides containing Trp (*48*) (E_{ox} = 1.0 V vs NHE) (*46*) and Tyr (*27*), providing precedence for the proposed oxidation of H3 Tyr41. During step 3, the H3 Tyr41 radical attacks the neighboring DNA to form H3−DNA cross-links. Previous investigations of DNA oxidation in short oligomers bound to tripeptides (*27*) and chromatin (*49*) have shown that tyrosine radicals generated in the proximity of DNA can form covalent adducts with T and C. Using gas chromatography and mass spectrometry, these adducts were characterized as having a carbon−carbon bond arising from attack of the tyrosyl radical (the C5-centered radical in Scheme 1) on the pyrimidine 5−6 double bond (*11*, *12*). Tyr−pyrimidine lesions are extremely stable at physiological temperatures in vivo since it takes 19 days for their levels to return to background in the renal cells of ferric nitrilotriacetate-treated Wistar rats (*41*). This stability is consistent with the stability measured for our DNA−H3 adducts at 37 °C (Figure 7). To be valid, this scheme requires that the rate of Tyr−pyrimidine cross-link formation in a NCP must be faster than the rate of the competing reaction between the phenoxyl radical and molecular oxygen (*50*).

Currently missing from this scheme is a rationalization for our observation of multiple DNA−protein cross-links in the SDS−PAGE EMSAs, Western blots, and Pol III footprinting of irradiated **rAQ-601**. In particular, the Pol III footprints show that three nucleobases are cross-linked to H3 in irradiated **rAQ-601** (Figure 6). Two scenarios can be

envisioned which would explain these findings. First, formation of a DPC between H3 Tyr41 and different pyrimidines could arise due to structural fluctuations at the PyB−H3 interface. Second, chemistry between multiple protein residues and the DNA nucleobases could be occurring. The amino acid residues surrounding H3 Tyr41 which are candidates for cross-linking include H3 Lys36 and H3 Lys37 since DNA−lysine cross-links have been observed in oxidized DNA−peptide complexes and NCPs (*26*, *51*). We are currently pinpointing the residues in H3 responsible for cross-linking using a combination of site-directed mutagenesis and mass spectrometry, and we intend to report the results of these studies in the near future.

Broader Impacts. There are three significant impacts of this research on our understanding of DNA−protein cross-linking during times of cellular oxidative stress. First, this study helps bridge two different literature observations. (i) Treatment of cells by low-dose ionizing radiation leads to the cross-linking of the core histones to DNA (*6*, *7*), and (ii) a common cross-linking chemistry involves the covalent attachment of Tyr to C or T residues in chromatin (*11*, *12*). The reasoning behind our assertion is outlined as follows. One of the direct products of ionizing radiation in aqueous solutions is OH•, an oxidant capable of generating C4′ radicals on the deoxyribose backbone (*52*). The work of Giese and co-workers (*53*) has shown that C4′ sugar radicals can oxidize neighboring nucleobases and initiate DNA CT. Therefore, since it appears that DNA CT is a likely outcome of cellular exposure to ionizing radiation, then the chemistry observed in this paper is a viable origin for the Tyr−pyrimidine cross-links found in chromatin.

The second impact is that this work establishes that the NCP region surrounding H3 Tyr41 is susceptible to DNA−protein cross-linking during times of oxidative stress. Since oxidative stress is manifested through the action of a wide variety of intracellular oxidants, we must recognize that DNA CT may not be the only source of DPCs involving H3 Tyr41 in vivo. One alternative pathway to the formation of a H3 Tyr41 radical involves the attack of OH• on the phenol side chain to form a dihydroxycyclohexadienyl radical (*54*), which then will spontaneously release water to form the resonance-stabilized Tyr radical shown in Scheme 1. While one might expect H3 Tyr41 to be buried in the DNA minor groove and thus protected from OH• attack, it must be remembered that there is a significant amount of breathing of the DNA away from the histone octamer surface, especially near the entrance to the nucleosome (*55*). These dynamic structural fluctuations may allow a wide variety of chemistries to occur in this region of the NCP with a finite, albeit low, probability.

Third, since we have mapped out the DNA region cross-linked to H3 in our experiments (PyB), we speculate that many known genomic NCP binding sequences will be susceptible to DPC formation arising from DNA CT. Segal et al. (*56*) recently deciphered a genomic code for NCP positioning which is consistent with a majority of the currently known NCP binding sequences in eukaryotic organisms. If one maps their code onto the 601 DNA sequence and NCP crystal structure (*36*), it is observed that the base pairs in contact with H3 Tyr41 are expected to be relatively G-rich as compared to the surrounding generic NCP positioning sequence. Therefore, DNA oxidation and any ensuing DNA CT are expected to lead to the oxidation of the nucleobases neighboring H3 Tyr41, thus sensitizing these NCPs to DNA−H3 cross-linking. Furthermore, this observation raises the possibility that genomic hot spots exist for DNA−histone cross-linking and that they may possess a dynamic nature due to chromatin remodeling events accompanying, for example, cell cycle progression and transcriptional regulation.

ACKNOWLEDGMENT

We thank Dr. Gerhard Munske (LBB1, Washington State University) for synthesizing the PCR primers, Wendy Smith for help performing the DNA footprinting experiments, Dr. Jonathan Widom (Northwestern University) for providing the 601 pGEM-3z plasmid, and Dr. Michael J. Smerdon (Washington State University), and Joseph N. Nichols for their critical reading of the manuscript and comments.

SUPPORTING INFORMATION AVAILABLE

DNA sequencing gels showing the OH• and ExoIII footprinting of **NH_2-601** and **rNH_2-601** (Figure S1), Pol III footprinting of ±UV **rNH_2-601** (Figure S2), and products of DNA CT in **rAQ-601** samples treated with trypsin to remove the histone tails (Figure S3). This material is available free of charge via the Internet at http://pubs.acs.org.

REFERENCES

1. Houstis, N., Rosen, E. D., and Lander, E. S. (2006) Reactive oxygen species have a causal role in multiple forms of insulin resistance, *Nature 440*, 944−948.
2. Kojda, G., and Harrison, D. (1999) Interactions between NO and reactive oxygen species: Pathophysiological importance in atherosclerosis, hypertension, diabetes and heart failure, *Cardiovasc. Res. 43*, 562−571.
3. Feig, D. I., Reid, T. M., and Loeb, L. A. (1994) Reactive oxygen species in tumorigenesis, *Cancer Res. 54*, 1890s−1894s.
4. Halliwell, B., and Gutteridge, J. M. C. (2000) *Free radicals in biology and medicine*, 3rd ed., Oxford Science Publications, Oxford, U.K.
5. Barker, S., Weinfeld, M., and Murray, D. (2005) DNA-protein crosslinks: Their induction, repair and biological consequences, *Mutat. Res. 589*, 111−135.
6. Barker, S., Weinfeld, M., Zheng, J., Li, L., and Murray, D. (2005) Identification of mammalian proteins cross-linked to DNA by ionizing radiation, *J. Biol. Chem. 280*, 33826−33838.
7. Mee, L. K., and Adelstein, S. J. (1981) Predominance of core histones in formation of DNA-protein crosslinks in γ-irradiated chromatin, *Proc. Natl. Acad. Sci. U.S.A. 78*, 2194−2198.
8. Matsumoto, A. (2000) Histone H3 and heat shock protein GRP78 are selectively cross-linked to DNA by photoactivated Gilvocarcin V in human fibroblasts, *Cancer Res. 60*, 3921−3926.
9. Miller, C. A., and Costa, M. (1989) Analysis of proteins cross-linked to DNA after treatment of cells with formaldehyde, chromate, and cis-diamminedichloroplatinum(II), *Mol. Toxicol. 2*, 11−26.
10. Cao, T. M., and Sung, M. T. (1982) Ultraviolet light induced preferential cross-linking of histone H3 to deoxyribonucleic acid in chromatin and nuclei of chicken erythrocytes, *Biochemistry 21*, 3419−3427.
11. Dizdaroglu, M., Gajewski, E., Reddy, P., and Margolis, S. A. (1989) Structure of a hydroxyl radical induced DNA-protein cross-link involving thymine and tyrosine in nucleohistone, *Biochemistry 28*, 3625−3628.
12. Gajewski, E., and Dizdaroglu, M. (1990) Hydroxyl radical induced cross-linking of cytosine and tyrosine in nucleohistone, *Biochemistry 29*, 977−980.
13. Seidel, C. A. M., Schulz, A., and Sauer, M. H. M. (1996) Nucleobase-specific quenching of fluorescent dyes. 1. Nucleobase one-electron redox potentials and their correlation with static and dynamic quenching efficiencies, *J. Phys. Chem. 100*, 5541−5553.

14. Boon, E. M., and Barton, J. K. (2002) Charge transport in DNA, *Curr. Opin. Struct. Biol. 12*, 320−329.
15. Joy, A., and Schuster, G. B. (2005) Long-range radical cation migration in DNA: Investigation of the mechanism, *Chem. Commun. 14*, 2778−2784.
16. Lewis, F. D., Letsinger, R. L., and Wasielewski, M. R. (2001) Dynamics of photoinduced charge transfer and hole transport in synthetic DNA hairpins, *Acc. Chem. Res. 34*, 159−170.
17. Giese, B. (2002) Electron transfer in DNA, *Curr. Opin. Chem. Biol. 6*, 612−618.
18. Henderson, P. T., Jones, D., Hampikian, G., Kan, Y., and Schuster, G. B. (1999) Long-distance charge transport in DNA: The phonon-assisted polaron-like hopping mechanism, *Proc. Natl. Acad. Sci. U.S.A. 96*, 8353−8358.
19. Nunez, M. E., Hall, D. B., and Barton, J. K. (1999) Long-range oxidative damage to DNA: Effects of distance and sequence, *Chem. Biol. 6*, 85−97.
20. Evans, M. D., Dizdaroglu, M., and Cooke, M. S. (2004) Oxidative DNA damage and disease: Induction, repair and significance, *Mutat. Res. 567*, 1−61.
21. Boon, E. M., Pope, M. A., Williams, S. D., David, S. S., and Barton, J. K. (2002) DNA-Mediated Charge Transport as a Probe of MutY-DNA Interaction, *Biochemistry 41*, 8464−8470.
22. Rajski, S. R., and Barton, J. K. (2001) How different DNA-binding proteins affect long-range oxidative damage to DNA, *Biochemistry 40*, 5556−5564.
23. Nunez, M. E., Noyes, K. T., and Barton, J. K. (2002) Oxidative charge transport through DNA in nucleosome core particles, *Chem. Biol. 9*, 403−415.
24. Nakatani, K., Dohno, C., Ogawa, A., and Saito, I. (2002) Suppression of DNA mediated charge transport by *BamHI* binding, *Chem. Biol. 9*, 361−366.
25. Bjorklund, C. C., and Davis, W. B. (2006) Attenuation of DNA charge transport by compaction into a nucleosome core particle, *Nucleic Acids Res. 34*, 1836−1846.
26. Perrier, S., Hau, J., Gaparutto, D., Cadet, J., Favier, A., and Ravanat, J.-L. (2006) Characterization of lysine-guanine cross-links upon one-electron oxidation of a guanine-containing oligonucleotide in the presence of a trilysine peptide, *J. Am. Chem. Soc. 128*, 5703−5710.
27. Wagenknecht, H.-A., Stemp, E. D. A., and Barton, J. K. (2000) DNA-bound peptide radicals generated through DNA-mediated electron transport, *Biochemistry 39*, 5483−5491.
28. Kurbanyan, K., Nguyen, K. L., To, P., Rivas, E. V., Lueras, A. M., Kosinski, C., Steryo, M., Gonzalez, A., Mah, D. A., and Stemp, E. D. C. (2003) DNA-protein cross-linking via guanine oxidation: Dependence upon protein and photosensitizer, *Biochemistry 42*, 10269−10281.
29. Lowary, P. T., and Widom, J. (1998) New DNA sequence rules for high affinity binding to histone octamer and sequence-directed nucleosome positioning, *J. Mol. Biol.*, 19−42.
30. Smith, C. L., and Petersen, C. L. (2005) A Conserved Swi2/Snf2 ATPase Motif Couples ATP Hydrolysis to Chromatin Remodeling, *Mol. Cell. Biol. 25*, 5880−5892.
31. Gasper, S. M., and Schuster, G. B. (1997) Intramolecular photoinduced electron transfer to anthraquinones linked to duplex DNA: The effect of gaps and traps on long-range radical cation migration, *J. Am. Chem. Soc. 119*, 12762−12771.
32. Libertini, L. J., and Small, E. W. (1980) Salt-induced transitions of chromatin core particles studied by tyrosine fluorescence anisotropy, *Nucleic Acids Res. 8*, 3517−3534.
33. Anderson, J. D., and Widom, J. (2000) Sequence and position-dependence of the equilibrium accessibility of nucleosomal DNA target sites, *J. Mol. Biol. 296*, 979−987.
34. Tullius, T. D., Dombroski, B. A., Churchill, M. E., and Kam, L. (1987) Hydroxyl radical footprinting: A high-resolution method for mapping protein-DNA contacts, *Methods Enzymol. 155*, 537−558.
35. Prunell, A. (1983) Periodicity of exonuclease III digestion of chromatin and the pitch of DNA on the nucleosome, *Biochemistry 22*, 4887−4893.
36. Davey, C. A., Sargent, D. F., Luger, K., Maeder, A. W., and Richmond, T. J. (2002) Solvent mediated interactions in the structure of the nucleosome core particle at 1.9 Å resolution, *J. Mol. Biol. 319*, 1097−1113.
37. Shao, F., O'Neill, M. A., and Barton, J. K. (2004) Long-range oxidative damage to cytosines in duplex DNA, *Proc. Natl. Acad. Sci. U.S.A. 101*, 17914−17919.
38. Joy, A., Ghosh, A. K., and Schuster, G. B. (2006) One-electron oxidation of DNA oligomers that lack guanine: Reaction and strand cleavage at remote thymines by long-distance radical cation hopping, *J. Am. Chem. Soc. 128*, 5346−5347.
39. Gale, J. M., and Smerdon, M. J. (1990) UV induced (6-4) photoproducts are distributed differently than cyclobutane dimers in nucleosomes, *Photochem. Photobiol. 51*, 411−417.
40. Quievryn, G., and Zhitkovich, A. (2000) Loss of DNA-protein crosslinks from formaldehyde-exposed cells occurs through spontaneous hydrolysis and an active repair process linked to proteosome function, *Carcinogenesis 21*, 1573−1580.
41. Toyokuni, S., Mori, T., Hiai, H., and Dizdaroglu, M. (1995) Treatment of Wistar rats with a renal carcinogen, ferric nitrilotriacetate, causes DNA-protein cross-linking between thymine and tyrosine in their renal chromatin, *Int. J. Cancer 62*, 309−313.
42. Bohm, L., Briand, G., Sautiere, P., and Crane-Robinson, C. (1981) Proteolytic digestion studies of chromatin core-histone structure. Identification of the limit peptides of histones H3 and H4, *Eur. J. Biochem. 119*, 67−74.
43. Polach, K. J., Lowary, P. T., and Widom, J. (2000) Effects of core histone tail domains on the equilibrium constants for dynamic DNA site accessibility in nucleosomes, *J. Mol. Biol. 298*, 211−223.
44. Li, G., and Widom, J. (2004) Nucleosomes facilitate their own invasion, *Nat. Struct. Mol. Biol. 11*, 763−769.
45. Zweidler, A. (1992) Role of individual histone tyrosines in the formation of the nucleosome complex, *Biochemistry 31*, 9205−9211.
46. DeFelippis, M. R., Murthy, C. P., Broitman, F., Weinraub, D., Faraggi, M., and Klapper, M. H. (1991) Electrochemical properties of tyrosine phenoxy and tryptophan indolyl radicals in peptides and amino acid analogs, *J. Phys. Chem. 95*, 3416−3419.
47. Steenken, S., and Jovanovic, S. V. (1997) How Easily Oxidizable Is DNA? One-Electron Reduction Potentials of Adenosine and Guanosine Radicals in Aqueous Solution, *J. Am. Chem. Soc. 119*, 617−618.
48. Wagenknecht, H.-A., Stemp, E. D. A., and Barton, J. K. (2000) Evidence of electron transfer from peptides to DNA: Oxidation of DNA-bound tryptophan using the flash-quench technique, *J. Am. Chem. Soc. 122*, 1−7.
49. Olinski, R., Nackerdien, Z., and Dizdaroglu, M. (1992) DNA-protein cross-linking between thymine and tyrosine in chromatin of γ-irradiated or H_2O_2-treated cultured human cells, *Arch. Biochem. Biophys. 297*, 139−143.
50. Dorfman, L. M., Taub, I. A., and Buehler, R. E. (1962) Pulse radiolysis studies. I. Transient spectra and reaction-rate constants in irradiated aqueous solutions of benzene, *J. Chem. Phys. 36*, 3051−3061.
51. Dizdaroglu, M., and Gajewski, E. (1989) Structure and mechanism of hydroxyl radical-induced formation of a DNA-protein cross-link involving thymine and lysine in nucleohistone, *Cancer Res. 49*, 3463−3467.
52. Dizdaroglu, M., Von Sonntag, C., and Schulte-Frohlinde, D. (1975) Strand breaks and sugar release by gamma-irradiation of DNA in aqueous solution, *J. Am. Chem. Soc. 97*, 2277−2278.
53. Giese, B. (2000) Long-Distance Charge Transport in DNA: The Hopping Mechanism, *Acc. Chem. Res. 33*, 631−636.
54. Land, E. J., and Ebert, M. (1967) Pulse radiolysis studies of aqueous phenol, *Trans. Faraday Soc. 63*, 1181−1190.
55. Polach, K. J., and Widom, J. (1995) Mechanism of protein access to specific DNA sequences in chromatin: A dynamic equilibrium model for gene regulation, *J. Mol. Biol. 254*, 130−149.
56. Segal, E., Fondufe-Mittendorf, Y., Chen, L., Thastrom, A., Field, Y., Moore, I. K., Wang, J.-P. Z., and Widom, J. (2006) A genomic code for nucleosome positioning, *Nature 442*, 772−778.

BI700475B